

A proton Computed Tomography based medical imaging system

To cite this article: M Scaringella *et al* 2014 *JINST* **9** C12009

View the [article online](#) for updates and enhancements.

You may also like

- [A binary readout chip for silicon microstrip detector in proton imaging application](#)
V. Sipala, M. Bruzzi, M. Bondi et al.
- [Proton Computed Tomography: iterative image reconstruction and dose evaluation](#)
C. Civinini, D. Bonanno, M. Brianzi et al.
- [A proton Computed Tomography system for medical applications](#)
V Sipala, M Bruzzi, M Bucciolini et al.



ECS
The
Electrochemical
Society
Advancing solid state &
electrochemical science & technology

DISCOVER
how sustainability
intersects with
electrochemistry & solid
state science research

10th INTERNATIONAL CONFERENCE ON POSITION SENSITIVE DETECTORS
7–12 SEPTEMBER 2014,
UNIVERSITY OF SURREY, GUILDFORD, SURREY, U.K.

A proton Computed Tomography based medical imaging system

**M. Scaringella,^{a,1} M. Bruzzi,^{b,c} M. Bucciolini,^{c,d,j} M. Carpinelli,^{h,i} G.A.P. Cirrone,^e
C. Civinini,^c G. Cuttone,^e D. Lo Presti,^{f,g} S. Pallotta,^{c,d,j} C. Pugliatti,^{f,g} N. Randazzo,^f
F. Romano,^e V. Sipala,^{h,i} C. Stancampiano,^e C. Talamonti,^{c,d,j} E. Vanzi^k and M. Zani^{c,d}**

^aDipartimento di Ingegneria dell'Informazione, Università di Firenze, Florence, Italy

^bDipartimento di Fisica e Astronomia, Università di Firenze, Florence, Italy

^cINFN — Sezione di Firenze, Florence, Italy

^dDipartimento di Scienze Biomediche, Sperimentali e Cliniche, Università di Firenze, Florence, Italy

^eINFN — Laboratori Nazionali del Sud, Catania, Italy

^fINFN — Sezione di Catania, Catania, Italy

^gDipartimento di Fisica e Astronomia, Università di Catania, Catania, Italy

^hDipartimento di Chimica e Farmacia, Università di Sassari, Sassari, Italy

ⁱINFN Sezione di Cagliari, Cagliari, Italy

^jSOD Fisica Medica, Azienda Ospedaliero-Universitaria Careggi, Firenze, Italy

^kFisica Sanitaria, Azienda Ospedaliero-Universitaria Senese, Siena, Italy

E-mail: scaringella@gmail.com

ABSTRACT: This paper reports on the activity of the INFN PRIMA/RDH collaboration in the development of proton Computed Tomography (pCT) systems based on single proton tracking and residual energy measurement. The systems are made of a silicon microstrip tracker and a YAG:Ce crystal calorimeter to measure single protons trajectory and residual energy, respectively.

A first prototype of pCT scanner, with an active area of about $5 \times 5 \text{ cm}^2$ and a data rate capability of 10 kHz, has been constructed and characterized with 62 MeV protons at INFN Laboratori Nazionali del Sud in Catania (Italy) and with 180 MeV protons at The Svedberg Laboratory (TSL) in Uppsala (Sweden). Results of these measurements, including tomographic reconstructions of test phantoms, will be shown and discussed.

An upgraded system with an extended field of view (up to $\sim 5 \times 20 \text{ cm}^2$) and an increased event rate capability up to one MHz, presently under development, will be also described.

KEYWORDS: Si microstrip and pad detectors; Instrumentation for hadron therapy

¹Corresponding author.

Contents

1	Introduction	1
2	The pCT scanner	2
3	Tomographic reconstruction	3
4	The upgraded pCT system	4
4.1	Silicon tracker	4
4.1.1	Silicon sensors	5
4.1.2	Front-end ASIC	5
4.1.3	Digital DAQ	5
4.1.4	Speed rate characterization	6
4.2	Calorimeter	7
5	Conclusions	7

1 Introduction

Proton radiation therapy is one of the most precise techniques for conformal radiation therapy in the treatment of cancer. One of the aspects that limits this medical approach is the relatively low accuracy of the stopping power (SP) maps inside the tissue, which are required for treatment planning and patient positioning, that today are derived from X-ray CT scans by converting the relative absorption coefficient (“Hounsfield values”) to SP [1]. The error introduced in this conversion, due to the differences in the physical interaction with matter between protons and photons, can be avoided by using protons to directly image the volume of interest. In this framework proton Computed Tomography (pCT) is an imaging technique based on the use of proton beams with kinetic energies of the order 200 MeV aimed to minimize the uncertainties of the reconstructed SP distributions.

A pCT system which aims to improve the accuracy on the SP map with respect to the ones obtained by conventional X-ray CT should be able to, at least partially, overcome the problems introduced by the intrinsic effect of the Multiple Coulomb Scattering (MCS) on charged particles crossing matter. A viable solution to this problem is to measure the trajectory of each proton both upstream and downstream the object under test. Having measured the trajectory entry and exit points and directions, the proton Most Likely Path (MLP) inside the phantom can be estimated [2, 3]. The energy loss along the proton path can then be extracted from the measurement of its residual energy. The data obtained from these measurements, taken at different angles with respect to the phantom, can then be processed through tomographic reconstruction algorithms to reconstruct the 3-dimensional SP maps of the phantom [4].

The PRIMA/RDH collaboration has developed a first pCT scanner prototype, based on single particle approach, with a field of view of $5 \times 5 \text{ cm}^2$ [5–10]. A description of this system, together with reconstruction of tomographic data, will be reported in section 2 and 3. An upgraded prototype with enlarged field of view ($5 \times 20 \text{ cm}^2$) and increased data rate capability (1 MHz) is now under development. The description of this new system will be reported in section 4.

2 The pCT scanner

A schematic of the pCT scanner is shown in figure 1.

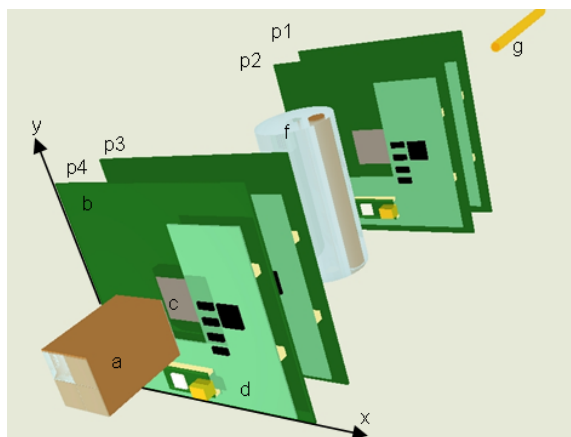


Figure 1. Schematic description of the pCT apparatus. The system components are the following: a) calorimeter; b) tracker front-end board; c) silicon microstrip sensor; d) tracker digital board; f) phantom; g) beam pipe; p1-p4) tracker planes.

The tracker is composed of four x-y planes, two upstream and two downstream the phantom. One x-y plane is made of two modules, each one carrying a silicon microstrip sensor, mounted piggy-back and rotated by 90° . Each sensor is mounted over a square aperture of a printed circuit board (front-end board) which also contains the front-end read-out chips. A second board (digital board), containing the digital read-out chain, local memory for data storage and an ethernet module for data transmission, is plugged onto the front-end board. The phantom is mounted on a rotating support that allows to acquire the projections at different angles needed for the tomographic reconstruction. The calorimeter is placed at the end of the proton path.

The sensors are $200 \mu\text{m}$ thick single-sided p-on-n silicon microstrip detectors. The total number of strips is 256 with $200 \mu\text{m}$ pitch for an active area of $5.1 \times 5.1 \text{ cm}^2$. The front-end read-out chip, designed in AMS $0.35 \mu\text{m}$ CMOS technology, consists of 32-channels, each equipped with a charge sensitive amplifier, a shaper and a comparator that produces a binary output by comparison with an external common threshold voltage. A fully parallel configuration has been implemented in order to maximize the read-out speed rate. The current pulse from the microstrip can be simulated, for test purposes and calibration, by applying a voltage step at the chip test terminal, which is AC coupled to the preamplifier input by an internal capacitance $C_t = 500 \text{ fF}$.

The calorimeter is made by four YAG:Ce (Yttrium Aluminum Garnet activated by cerium) scintillating crystals assembled in a 2×2 matrix. The material has been chosen because of its short light decay constant (70 ns) that allows its use in high particle rate conditions. Each crystal has a $3 \times 3 \text{ cm}^2$ section and a depth of 10 cm sufficient to stop a 230 MeV kinetic energy proton. Each crystal is glued to a S3204 commercial photodiode read out by a charge-sensitive amplifier and a shaper with a peak time of $1 \mu\text{s}$. The remaining surface of the crystal is covered by a thin reflective mylar layer to prevent light leakage. The analog signals are sampled and digitally converted by a commercial acquisition board at 14 bit and 10 MHz. Each analog signal is also sent to a comparator, the logical or of the four outputs is used by the whole system for triggering.

A picture of the system mounted on the CATANA beam line is shown in 2.



Figure 2. picture of the PRIMA/RDH pCT scanner mounted at the CATANA beam line.

3 Tomographic reconstruction

The pCT system has been used to acquire tomographic data with 62 MeV protons at the CATANA beam line. The phantom was a polymethyl methacrylate (PMMA) cylinder (20 mm diameter and 40 mm length) with two coaxial off-axis holes of 4 and 6 mm diameters and 20 mm length (figure 3). A set of 36 projections at 10° steps with an average of 950000 events per projection have been acquired. The Filtered Back-Projection (FBP) algorithm has been applied for the tomographic reconstruction using a Butterworth filter with a cut-off frequency of 20/128 of the Nyquist frequency and different orders, a detailed description can be found in [12]. As an example figure 3 (a) shows the reconstructed images related to two slices, one in the uniform part and one in the area with the holes, obtained without cuts on data. In this case a 4 order filter was used and a spatial resolution (FWHM) of 0.9 mm with a 2.4% electron density resolution was obtained. Increasing the filter order the noise decreases but the spatial resolution gets worse (figure 3 (b)).

The main advantage of the FBP algorithm is that the computational time is very low, as an example in this case the entire volume reconstruction took 22 s on a standard PC. One of the limits of this approach is that the FBP approach is based on the hypothesis of straight line for the particle path, in our case only information of two of the tracker planes were used (one upstream and

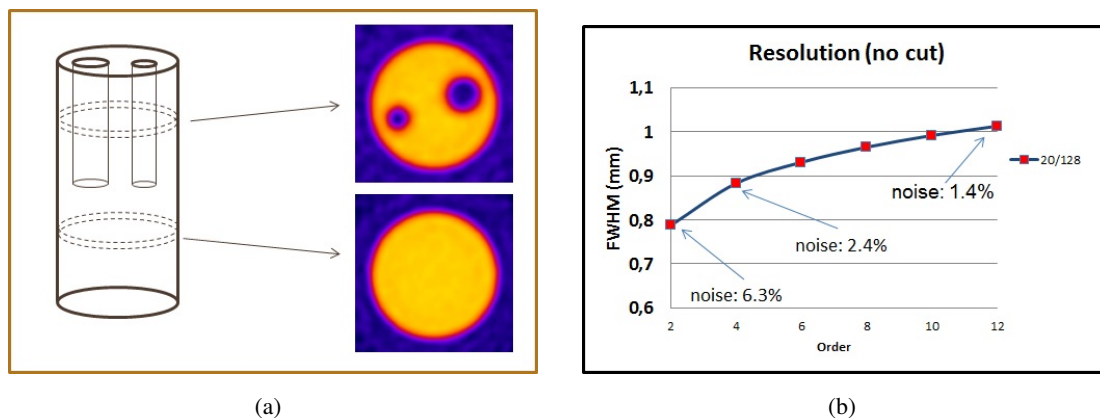


Figure 3. (a) Sketch of the analyzed phantom (left), FBP tomographic reconstruction images for two slices: one in the uniform part and one in the area with holes (right). (b) Plot of spatial resolution vs filter order.

one downstream the phantom). More suitable algorithms based on Algebraic Reconstruction Technique (ART) [13] that use the calculated MLP for the proton path are under development within the collaboration. Anyway FBP reconstruction proved to give a satisfactory image quality and can be considered a useful tool in proton imaging to obtain a first assessment of the image when computational speed is important, for example for patient positioning, and to provide a starting point of iterative algorithms based on ART.

The system has also been characterized with 180 MeV at TSL, results are reported in [10, 14].

4 The upgraded pCT system

In order to meet the requirements for a pre-clinical test phase in terms of phantom size and particle rate a new prototype has been designed and is now under construction. The field of view of this new prototype will be $5 \times 20 \text{ cm}^2$ and the acquisition event rate will be increased up to 1 MHz. The rectangular shape has been chosen to be able to image objects of clinical interest (e.g. a human head) by dividing the tomography in slices.

4.1 Silicon tracker

The tracker is again composed of four x-y planes, two upstream and two downstream the phantom. Each plane contains eight silicon microstrip sensors, 4 for the horizontal (x-side) and 4 for the vertical (y-side) coordinates. The sensors are glued over a rectangular aperture on both sides of a printed circuit board that also hosts the front-end chips and the digital readout electronics. On both sides the sensors are placed one next to the other with a slight superposition ($\sim 2.75\%$ of the sensing area) in order to avoid dead zones.

On the x side each of the four sensors has a dedicated read-out unit composed of a group of eight 32-channel parallel binary front-end ASICs and a Xilinx Spartan 6 FPGA (called slave FPGA). On the y-side the strips are daisy-chained between two couple of sensors so that the acquisition is divided in two read-out units giving a total number of 6 read-out units per plane.

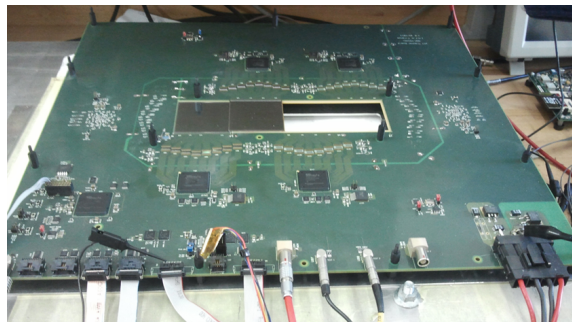


Figure 4. Picture of the tracker board of the upgraded prototype.

The first board has been produced and loaded with all the digital components, 4 sensors (2 on x-side and 2 on the y-side) and the related front-end chips. A picture of the board is reported in figure 4.

4.1.1 Silicon sensors

The silicon sensors are very similar to the ones used in the first prototype except for the thickness which has been increased to $320\ \mu\text{m}$ to improve signal to noise ratio for longer strips. Simulations have been carried out to estimate the error on the MLP due to the MCS in the silicon for this thickness value showing that this contribution is negligible compared to the error due to the MCS in the phantom even in the overlap regions [15]. The preliminary characterization of the 36 sensors that have been procured showed a depletion voltage around 85 V, an average current of $2.5\ \text{nA/cm}^2$ at full depletion and no bad strips over a total of 9216.

4.1.2 Front-end ASIC

A new front-end ASIC has been designed to improve the gain uniformity along the channel with respect to the first prototype. In particular for each channel an integrated 8 bit DAC has been introduced to finely tune the threshold voltage for the output comparator. An I²C slave interface has also been enclosed to set the DAC values channel by channel.

4.1.3 Digital DAQ

On a plane level the digital DAQ chain is composed of the 6 slave FPGAs, one for each read-out unit, and one master FPGA (Xilinx Spartan 6) that receives the data related to an event from the slave FPGAs when a trigger occurs, performs a first level event building and sends the data to the central DAQ unit. The communication between each slave and the master FPGAs is made through a serial data link on a 8-bit LVDS data bus at 1.6 Gbps. The central DAQ unit of the whole system is a Xilinx Virtex 6 based board that receives the data from the four planes, performs a second level event building and sends the data to the host PC through an ethernet based communication. Also the communication between the central DAQ and each of the four master FPGAs is based on a serial link at 1.6 Gbps through a 8 bit LVDS bus that goes on a twisted-pair flat cable. Each slave FPGA continuously samples the level of all channels at 50 MHz and updates the event related information (duration and delay) in a $2.56\ \mu\text{s}$ sampling time window across the trigger (128 samples, 21 before

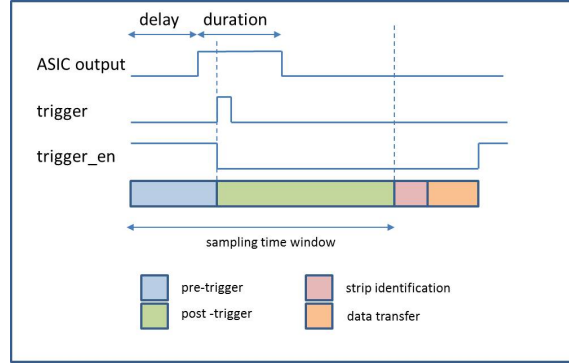


Figure 5. Diagram of the acquisition operation in the slave FPGA.

the trigger, 107 after, figure 5). When a trigger occurs the acquisition in the slave FPGAs starts and the trigger is disabled. After the sampling time windows has expired the active strips are identified and the corresponding information is stored in a temporary buffer, finally the data are sent to the master FPGA and the trigger is enabled again. A header is attached to each event data set containing a timestamp, an event number and a 7 bit tag (global event number) that comes from the calorimeter read-out unit and is used for synchronization purposes. The hit finding is done through a priority encoder which takes a number of clock cycles equal to the number of active strips per event plus one of latency. In most cases one or two strips per event are expected for each sensor [10], as an example for a two strip event the hit finding completes in 60 ns while the transmission takes around 100 ns.

The master FPGA has one FIFO buffer for each readout unit so that data processing and transmission to the central central unit can be done in parallel with data acquisition. The Virtex 6 FPGA in the central unit contains a double FIFO that acts as a ping pong buffer so that while one of the FIFOs is full data are written to an on board DDR3 RAM through burst transfer while the other FIFO is written. Since the burst transfer is faster than the estimated write speed, data can be transferred continuously without introducing dead time. An embedded processor (Microblaze) is implemented in the Virtex 6 to handle DDR3 and ethernet peripherals.

4.1.4 Speed rate characterization

In the present configuration the time needed to complete the acquisition of an event is clearly dominated by the width of the sampling time window which limits the maximum achieved speed rate to ~ 300 kHz. In order to reach a particle rate of 1 MHz the sampling the time window has to be reduced in order to keep the total acquisition time below $1 \mu\text{s}$. In order to estimate the minimum width for the time window, we performed calibration tests by injecting a known charge into the calibration capacitance of all channels of a read-out unit using a pulse generator. The charge values expected in beam data have been calculated through GEANT4 simulations for a minimum and maximum proton energy, expected in a clinical imaging application, of 60 and 200 MeV respectively. The minimum expected charge for 200 MeV protons is $25.6 ke^-$, the most probable charge for 60 MeV is $153.6 ke^-$. Using the most probable value of the charge instead of the maximum is not expected to influence this calculation since at these charge values the duration saturates for our

Table 1. Mean value and standard deviation for the duration and delay distribution over 256 channels of a read-out unit.

injected charge [ke^-]	duration [ns]		delay [ns]	
	μ_{duration}	σ_{duration}	μ_{delay}	σ_{delay}
25.6	268	34	530	36
51.2	320	32	480	30
153.6	360	32	440	28

chip. The mean value and standard deviation of the delay and duration distributions for 25.6, 51.2 and 153.6 ke^- are reported in table 1.

Starting from these values it is possible to calculate the minimum time window that allows to correctly record all the events within 3σ confidence which is 640 ns. Considering also the time spent in the hit finding and transmission phases in the case of a two strips event (~ 160 ns) the sampling time window could be reduced down to 800 ns which translates in a maximum instantaneous acquisition rate of 1.25 MHz.

4.2 Calorimeter

The calorimeter is made of 14 of the same YAG:Ce crystals of the first prototype placed in a 2×7 array to cover a 6×21 cm² active area. Each crystal is glued on a 18×18 mm² commercial silicon photodiode read out by a pre-amplifier and shaper circuit. The 14 analog channels are then sampled and converted to digital by a NI-5751 module at 5 MHz with 14 bit resolution. The digitized data are then processed to produce the trigger signal for the entire system and to generate the global event number that is used to synchronize the event data between tracker and calorimeter.

5 Conclusions

The PRIMA/RDH collaboration has built a pCT scanner based on a microstrip silicon tracker and a YAG:Ce crystal calorimeter with a field of view of 5×5 cm². Tomographic data have been acquired with 62 MeV proton beam and reconstructed with the FBP algorithm showing a good performance of the device. An upgraded prototype with enlarged field of view (5×20 cm²) and a data rate capability of 1 MHz is now under construction.

References

- [1] B. Schaffner and E. Pedroni, *The precision of proton range calculations in proton radiotherapy treatment planning: experimental verification of the relation between CT-HU and proton stopping power*, *Phys. Med. Biol.* **43** (1998) 1579.
- [2] D.C. Williams, *The most likely path of an energetic charged particle through a uniform medium*, *Phys. Med. Biol.* **49** (2004) 2899.
- [3] R.W. Schulte et al., *A maximum likelihood proton path formalism for application in proton computed tomography*, *Med. Phys.* **35** (2008) 4849.

- [4] T. Li et al., *Reconstruction for proton computed tomography by tracing proton trajectories: a Monte Carlo study*, *Med. Phys.* **33** (2006) 699.
- [5] G.A.P. Cirrone et al., *The Italian project for a proton imaging device*, *Nucl. Instrum. Meth. A* **576** (2007) 194.
- [6] V. Sipala et al., *A proton imaging device: design and status of realization*, *Nucl. Instrum. Meth. A* **612** (2010) 566.
- [7] C. Cividini et al., *Towards a proton imaging system*, *Nucl. Instrum. Meth. A* **623** (2010) 588.
- [8] C. Talamonti et al., *Proton radiography for clinical applications*, *Nucl. Instrum. Meth. A* **612** (2010) 571.
- [9] D. Menichelli et al., *Characterization of a Silicon Strip Detector and a YAG:Ce Calorimeter for a Proton Computed Radiography Apparatus*, *IEEE Trans. Nucl. Sci.* **57** (2010) 8.
- [10] M. Scaringella et al., *The PRIMA (PRoton IMAGING) collaboration: development of a proton computed tomography apparatus*, *Nucl. Instrum. Meth. A* **730** (2013) 178.
- [11] J. Allison et al., *Geant4 developments and applications*, *IEEE Trans. Nucl. Sci.* **53** (2006) 270.
- [12] E. Vanzi et al., *The PRIMA collaboration: Preliminary results in FBP reconstruction of pCT data*, *Nucl. Instrum. Meth. A* **730** (2013) 184.
- [13] R. Gordon, R. Bender and G. Herman, *Algebraic Reconstruction Techniques (ART) for three-dimensional electron microscopy and X-ray photography*, *J. Theor. Biol.* **29** (1970) 471.
- [14] C. Talamonti et al., *PRIMA Proton Imaging for Clinical Application*, *IEEE Nucl. Sci. Symp. Med. Imag. Conf. Rec.* **2012** (2012) 2218.
- [15] C. Cividini et al., *Recent results on the development of a proton computed tomography system*, *Nucl. Instrum. Meth. A* **723** (2013) 573.